# Growth-Induced Wrinkles and Dotlike Patterns of a Swollen Fluoroalkylated Thin Film by the Reaction of Surface-Attached Polymethylhydrosiloxane

Thierry Thami, Michel Ramonda, Lynda Ferez, Valérie Flaud, Eddy Petit, Didier Cot, Bertrand Rebière, Bruno Ameduri

# Growth-Induced Wrinkles and Dots-like Patterns of a Swollen Fluoroalkylated Thin Film by Reaction of Surface-Attached Polymethylhydrosiloxane

| | |
|---|---|
| Journal: | *Langmuir* |
| Manuscript ID | la-2022-02109j.R1 |
| Manuscript Type: | Article |
| Date Submitted by the Author: | n/a |
| Complete List of Authors: | Thami, Thierry; University of Montpellier, Institut Européen des Membranes<br>Ramonda, Michel; Centrale de Technologie en Micro et Nanoélectronique<br>Ferez, Lynda; University of Montpellier, Institut Européen des Membranes<br>Flaud, Valerie; Universite de Montpellier, Institut Europeen des Membranes<br>Petit, Eddy; University of Montpellier, IEM<br>Cot, Didier; Institut Europeen des Membranes, Université Montpellier 2<br>Rebière, Bertrand; Université de Montpellier, Institut Européen des Membranes<br>Ameduri, Bruno; University of Montpellier, Institut Charles Gerhardt |
| | |

1

# Growth-Induced Wrinkles and Dots-like Patterns of a Swollen Fluoroalkylated Thin Film by Reaction of Surface-Attached Polymethylhydrosiloxane

Thierry Thami[1]*, Michel Ramonda[2], Lynda Ferez[1], Valérie Flaud[3], Eddy Petit[1], Didier Cot[1], Bertrand Rebière[3], Bruno Ameduri[3]**

[1] Institut Européen des Membranes, IEM, Univ Montpellier, CNRS, ENSCM, Montpellier, France

[2] Centre de technologie de Montpellier, CTM, Univ Montpellier, Bât. 5, cc007 Campus Saint Priest, Montpellier, France

[3] Institut Charles Gerhardt de Montpellier, ICGM, Univ Montpellier, CNRS, ENSCM, Montpellier, France

Correspondence to: T. Thami (thierry.thami@umontpellier.fr)

Shared correspondence to: B. Ameduri (bruno.ameduri@enscm.fr)

## ABSTRACT

The design of hydrophobic surfaces requires a material which has a low solid surface tension and a simple fabrication process for anchoring and controlling the surface morphology. A generic method for spontaneous formation of robust instability patterns is proposed through the hydrosilylation of fluoroalkene bearing dangling chains, $R_f = C_6F_{13}(CH_2)_3$-, with soft polymethylhydrosiloxane (PMHS) spin-coated gel polymer (0.8 μm thick) using Karstedt catalyst. These patterns were easily formed by irreversible swelling reaction due to the attachment of layer to various substrates. The buckling instability was created by two different approaches for a gel layer bound: to a rigid silicon wafer substrate (A) and to a soft non-swelling silicone elastomer foundation (B). The observations of grafted $R_f$-PMHS films in the swollen state by microscopy revealed two distinct permanent patterns onto various substrates dot-like (A) / or wrinkle (B) of wavelength ($\lambda$ = 0.4–0.7 μm) / or ($\lambda$ = 4–7 μm). The elastic moduli ratios of film/substrate were determined using PeakForce Quantitative Nanomechanical Mapping. The characteristic wavelengths ($\lambda$) of the patterns for the systems (A) and (B) were quantitatively estimated in relation with the thickness of the top layer. A diversity of wrinkle morphologies can be achieved by grafting different side chains on pristine PMHS films. The water contact angle (WCA) hysteresis of fluorinated chain ($R_f$) was enhanced upon roughening the surfaces giving highly hydrophobic surface properties for water with static/hysteresis WCA of 136°/74° in the resulting wrinkle (B) and 119°/41° in dot-like (A) of lower roughness. The hydrophobic properties of grafted films on (A) with various mixtures of hexyl/fluoroalkyl chains were characterized by static CA: WCA 104°–119°, ethylene glycol CA 80°–96° and *n*-hexadecane CA 17°–61. A very low surface energy of 15 mN/m for $R_f$-PMHS was found on the smoother dot-like pattern.

**KEYWORDS** Fluorinated silicones; Hydrosilylation; PMHS; Sol-gel process; Solid surface energy; Swollen polymer; Wrinkled surface.

## 1. Introduction

Fluoropolymer-based systems are well-known for their ability to influence the surface properties of a material such as wettability, adhesion, friction, thermostability and they have many applications[1,2] in self-cleaning,[3–5] water pollution,[6] water and oil repellent fabrics,[7,8] microfluidic devices acting as barrier coating to organic solvent,[9] surface increasing hydrophobicity of silicone elastomers,[10,11] anti-icing,[12] anti-fogging[13] and moulding.[14] Fluorinated surface is an obvious choice for hydrophobic applications due to their ultra-low surface energy.[8,15–17] The wetting at solid and liquid interfaces is governed by surface chemistry and surface roughness.[18] A number of artificial superhydrophobic microstructured surfaces has been fabricated and functionalized to increase hydrophobicity either by trapping air at solid interface[19–22] or by infusing a lubricant liquid to create a repelling liquid interface.[23–25] The most commonly used surface coupling reagents are trichloro and triethoxy fluoroalkyl functional silanes,[26,27] fluorosilicones bearing reactive group for surface modification[17,28] and fluoroalkyl polyhedral oligomeric silsesquioxane (F-POSS).[29]

There are different ways to prepare hydrophobic rough surface[19] consisting to roughen the low-surface-energy material or to modify the rough surface of substrate with low-surface energy modifier through covalent bonding to afford stable structure. The spontaneous wrinkled formation on polymer surfaces[30,31] is also one other route for producing superhydrophobic surfaces[32] in combination with low-surface energy materials.[33] The wrinkled formation, in particular, is a strategy which has been developed to produce microstructured surface in the submicrometer range[34–37] using bilayers system composed of a rigid layer anchored on a soft plastic substrate. Such artificial wrinkling is generally based on elastic surface instabilities and buckling effect[38] due to compressive stress in soft crosslinked

polymer including hydrogel materials,[39–49] solvent-responsive films[50–54] and elastomers.[55–57] By taking advantage of this phenomena, wrinkling of soft polymer surfaces and other alternatives have been developed to fabricate buckled structures involving various strategies[30,58] mostly consisting in swelling, drying, heating or mechanical stretching/compression. Permanent wrinkling pattern can be achieved and stabilized through diffusion and polymerization of reactive liquid monomers by silane infusion based wrinkling in poly(2-hydroxyethyl methacrylate) (PHEMA).[54] Other methods have been described to obtain spontaneous robust patterns associating the very low surface energy of fluorinated polymer and self-wrinkling. Photopolymerizable fluoropolymer films[59–61] on rigid substrates, or fluoropolymer ($CF_x$) soft skin layer obtained by $CHF_3$ plasma treatment[62,63] were used to produce wrinkles.

We have recently reported the development of a simple and general method for the preparation of functional coatings on solid supports with well-characterized functionalities and surface properties for various applications.[64–67] Functional poly(methylhydrosiloxane) (PMHS), rich in Si–H groups, have been covalently anchored using sol-gel procedure giving in one step soft elastomeric gel bound *via* SiOSi linkages.[68] Sol-gel coating are advantageous over silanization for modification of solid surface due to the high density and homogenous film deposition. These Si–H functional layers were swollen by hydrosylilation grafting with hydrocarbon side chains as measured by ellipsometry.[64] The phenomenon may have potential in advanced micro-structuration of surface when the control of wetting properties is required.

The use of fluorinated compounds in combination with self-wrinkling induced by irreversible swelling reaction of polymer surfaces was not described before. In this study, the grafting of alkyl chains *via* hydrosilylation into crosslinked substrate bound PMHS films is proposed to create robust wrinkled patterns. Silicone gel containing perfluoroalkyl moieties were prepared

as powder by hydrolysis and polycondensation using trialkoxysilanes.[69] The synthesis of hybrid fluorinated silicones has been achieved in three steps by hydrosilylation, hydrolysis and polycondensation yielding fluorinated polysiloxanes of high thermal stability.[70] Fluorinated polysiloxane coatings with pendant fluoroalkyl side chains[71,72] have been synthesized by hydrosilylation of olefins onto linear PMHS $(CH_3HSiO)_p$. We proposed here a generic approach for permanent pattern creation originally using the driving force of the swelling phenomena by grafting side chains into the surface–bound crosslinked PMHS top surface (Figure 1). The introduction of hydrocarbon or fluorinated side chains by functionalization can act as a ‘‘solvent casting’’ for the polymer backbones, which induces a swollen structure where the polysiloxane segments become more extended in the functionalized network. The surface attachment of the bottom of thin films on substrates is also one of the keyfactor to obtain instability patterns due to swelling.

In this manuscript, permanent structured-surfaces on both silicon wafer and silicone elastomer substrates were achieved in two steps by applying PMHS spin-coated films using sol-gel process catalyzed by triflic acid, an efficient catalytic system for the polycondensation of polyorganosiloxane,[73] and in turn for the surface attachment on the films onto SiOH surface groups of substrates. In the second step, the substrate-anchored PMHS coating was functionalized in organic solvent by hydrosilylation of two molecules, 1*H*, 1*H*, 2*H*, 3*H*, 3*H*-tridecafluorononon-1-ene and 1-hexene. Acetonitrile was used to overcome the swelling issues of silicone elastomer substrates. We have chosen the preparation method for the engineering of hydrophobic surfaces based on the microstructuration and have studied the pattern formation resulting in buckling instability after grafting hydrocarbon or perfluoroalkyl chains. The characteristic parameters of the microstructured films are highlighted by applying two distinct physical approaches for films constrained on rigid or soft substrates. The molecular features of the functionalized and structured polysiloxane films were characterized by X-ray

Photoelectron Spectroscopy (XPS), Energy Dispersive X-ray (EDX) and infrared spectroscopies. Their elastic mechanical properties and topography were examined by PeakForce Quantitative Nanomechanical Mapping, while the wetting properties of the patterned surfaces were characterized by water contact angle (WCA) hysteresis measurements, and static CA in three solvents (water, ethylene glycol and *n*-hexadecane).

## 2. Material and Methods

### 2.1. Chemicals

Methyldiethoxysilane $HSi(CH_3)(OCH_2CH_3)_2$, triethoxysilane $HSi(OCH_2CH_3)_3$, 1-hexene $CH_3(CH_2)_3CH=CH_2$, triflic acid $CF_3SO_3H$ and Karstedt catalyst [$Pt_2$(*sym*-tetramethyldivinyldisiloxane)$_3$] (2–3 wt% Pt concentration in xylene) were purchased from Sigma-Aldrich, and used as received. *1H, 1H, 2H, 3H, 3H*-tridecafluoronon-1-ene $C_6F_{13}CH_2CH=CH_2$ was prepared *via* a two-step process.[74] Briefly, perfluorohexyl iodide $C_6F_{13}I$ (Atofina, Pierre Bénite, France) was reacted with allyl acetate through a free-radical reaction initiated with benzoyl peroxide followed by deiodoacetalization with activated zinc. The allyl perfluorinated olefin was distilled under reduced pressure as a colorless liquid (b.p. 49-51 °C/24 mmHg). Purity assessment of the product was characterized by $^1H$ and $^{19}F$ NMR spectroscopies. Allyl methoxy triethylene glycol ether $CH_3O(CH_2CH_2O)_3CH_2CH=CH_2$ was purchased from ABCR. Water for substrate cleaning was obtained from a Milli-Q water purification apparatus (Millipore). All solvents, ethanol, methanol, isopropanol, toluene, cyclohexane and acetonitrile, of synthesis grade purity, were purchased from Sigma-Aldrich. Toluene and cyclohexane were dried and distilled with calcium hydride before use. EtOH and $CH_3CN$ were used as received and dried over 4 Å molecular sieves. The solvents for contact angle measurements were Milli-Q water, ethylene glycol and *n*-hexadecane (Aldrich). The organic solvents of synthesis grade purity were used as received. Silicon wafers Si(100)

(ACM, France) in the form of native oxide layer and silicone rubber sheet materials were used and cut into smaller square strips of $2 \times 2$ cm$^2$. Commercially available poly(dimethylsiloxane) PDMS-based elastomer was purchased in the form of elastomer kit Med-4750 (Nusil) and procedure of fabrication by moulding into sheets of 0.22 mm thick (Statice, Besançon, France).

### 2.2. Thin Films Preparation

The preparation of 5% crosslinked pristine H-PMHS thin films on flat substrates is described elsewhere[64] by spin-coating of sol-gel solution of methyldiethoxysilane and triethoxysilane (5%) as a crosslinker. A similar procedure was used to prepare films on (100) silicon wafer (A) and on silicone elastomer Med-4750 (B) pieces. Alkylation of H-PMHS films on various substrates was achieved by hydrosilylation of *1H, 1H, 2H, 3H, 3H*-tridecafluorononon-1-ene and 1-hexene using Karstedt catalyst. Details of sample preparations are given in Supporting Information. For Atomic Force Microscopy (AFM) and electronic microscopy (*Vide infra*), 5 mm × 5 mm pieces were cut and mounted on metallic coins using an epoxy adhesive. The sample films on silicone Med-4750 sheet were removed from the glass slide, freeze fractured with liquid nitrogen (for cross-sectional view).

### 2.3. IR Spectroscopy

The Fourier-transform infrared (FTIR) spectroscopy in transmission mode was used to characterize the results of hydrosilylation on surface-coated silicon wafer. IR spectroscopy measurements were carried out on a Nicolet Nexus FTIR spectrometer in the 4000–400 cm$^{-1}$ range with a resolution of 4 cm$^{-1}$ and 32 scans were collected for each sample. A background spectrum was recorded in air prior to each sample using a piece of bare silicon wafer.

### 2.4. Attenuated Total Reflectance-Infrared Spectroscopy (ATR-FTIR)

ATR-FTIR spectra were recorded on a Nicolet Nexus FTIR spectrometer using an ATR accessory Durasampl*IR* II (diamond crystal, single-bounce beam path, 45° angle of incidence, 32 scans, 4 $cm^{-1}$ resolution). A baseline correction was applied to all spectra from 650 to 4000 $cm^{-1}$ prior to an ATR correction. A refractive index of 1.40 was taken for both coating and substrate of silicone elastomer Med-4750 (bare sheet) by assuming they have the same refractive index which is close to that of PDMS $[SiO(CH_3)_2]_p$.[75]

### 2.5. Assessment of Pristine PMHS Thickness from IR Spectra

The H-PMHS samples on Si wafer (A) were placed perpendicularly to the beam so that the recorded spectrum reflects the absorbance of the pristine thin film of thickness $h_0$, assuming the IR absorption spectrum follows equation eq. S1 similar to that of Beer–Lambert law.[76] The value of absorption coefficient ($\alpha$) of 0.27 $\mu m^{-1}$ for the Si–H stretching vibration at 2169 $cm^{-1}$ was calibrated from the peak absorbance of a 200-nm thick film for which independent ellipsometric thickness was easily determined (Estimated accuracy of ± 5%). The calibration was confirmed in the micrometer range from the cross section using scanning electron microscopy. For sample on silicone (B), $h_0$ was evaluated from absorbance of stretching Si-H band in corrected ATR-FTIR spectra (Supporting Information).

### 2.6. Ellipsometry

The thickness and refractive index of the pristine H-PMHS layer onto silicon wafer were measured using a Horiba Jobin Yvon PZ2000 ellipsometer equipped with a 632.8 nm He-Ne laser with a spot size of 2 mm.[64,68] The incidence angle was 70.0°. The refractive index of H-PMHS of 1.40 was found. Then, refractive indices used to calculate the H-PMHS thickness were 1.457 and 3.871–0.016*i* for native silicon oxide $SiO_2$ and silicon.[64]

### 2.7. Scanning Electron Microscopy (SEM)

SEM and cross-sectional view images were obtained with a Hitachi S-4800 instrument operating at an accelerating voltage of 2 kV, and with magnifications from of 1k × to 25k ×. The surfaces were prepared by coating an ultrathin (10 Å) very fine-grain platinum metal of high wettability.

### 2.8. Energy Dispersive X-ray Spectroscopy (EDX)

The weight / atomic percentages in the samples were determined by EDX using a Zeiss SEM EVOHD15 at 12 kV with the Oxford instruments software. Samples were deposited on double-sided carbon tape. The elemental composition in EDX analysis corresponds to probed depths of around 2–3 μm.

### 2.9. X-ray Photoelectron Spectroscopy (XPS)

XPS data were obtained on an ESCALAB 250 (Thermo Electron, UK) spectrophotometer using Al Kα (1486.6 eV) irradiation source (15 kV, 100 W). The acceleration tension and power of X-ray source were 15 kV and 100 W, respectively. The electron take-off angle was 90° at normal incidence of the sample surface. The samples were analyzed under ultra-high vacuum in the $10^{-9}$ mbar range. The spot size was approximately 400 $\mu m^2$. The composition in XPS analysis corresponds to depths of 5–10 nm. Survey scans (0–1350 eV) at low resolution were performed to identify the constitutive elements. High resolution C1s, Si2p, O1s, and F1s spectra were recorded to quantify elements present at the surface and to determine their chemical environment. The peaks were fitted with Gauss–Lorentz curves with

the theoretical sensitivity factors reported by Scofield.[77] A charge correction was applied to set the binding energy scale.

### 2.10. Surface Characterization by Optical Microscopy

Morphologies of the silicone Med-4750 samples supported on microscope glass slide were observed in transmission mode using a Bresser LCD Student Microscope (Magnification 500×) with 40× objective.

### 2.11. PeakForce Quantitative Nanomechanical Property Mapping (PF-QNM)

The mechanical characterization was performed with a Multimode AFM instrument (Bruker Corporation, USA) upgrade with Nanoscope V using PF-QNM imaging mode. A Bruker-ScanAsyst-Air probe equipped with a spring constant of the lever of 0.5 N/m (calculated with thermal tune) was used for sample measurements. After a first step to calibrate sensitivity deflection and sync distance QNM on a sapphire sample (Bruker Instruments), these values were confirmed during measurement on PDMS-Soft-1 (2.5 MPa) and on PDMS-Soft-2 (3.5 MPa) from Bruker, providing a tip radius of 40 nm to obtain indentation modulus in a good agreement using the well-known Johnson-Kendall-Roberts (JKR) model.[78] The applied maximum load was set at 20 nN for all the measurements while the peak force amplitude was set at 150 nm. The obtained force versus separation curves were analyzed in real time to obtain different mechanical properties: adhesion force, elastic modulus, deformation and energy dissipation. The JKR contact model was used to fit retract curve to calculate indentation JKR modulus (Poisson ratio was assumed to be 0.4 for all sample surfaces: PDMS, pristine and modified H-PMHS). These values were then sent to different data channels which are shown as a set of different images simultaneously with the topography image.

### 2.12. Contact Angle Measurement

Static and dynamic contact angle measurements with water were performed using GBX drop analysis system Digidrop (GBX, France). The static contact angle (CA) was performed by the sessile drop method with drop of volume (3 µL). CA was calculated by averaging the two CAs of the droplets, for at least three droplets deposited in different areas of the surface. The advancing CA ($\theta_{adv}$) and the receding CA ($\theta_{rec}$) were measured using the injection and the withdrawn of a 5 µL water droplet by using a motor-driven syringe at constant speed (0.5 µl/min). The static CA of *n*-hexadecane, ethylene glycol and water were measured to evaluate the solid surface energy by the method described by Owens and Wendt[79] (Supporting Information). All measurements were performed in air at ambient room temperature. The images of drop were analyzed by software (Visiodrop, GBX) by using an automated polynomial fitting method.

## 3. Results and Discussion

### 3.1. Preparation and Characterization of Dots-like and Wrinkles Micro-patterns

#### 3.1.1. *Strategy for Spontaneous Pattern Formations*

Micro-structured thin films of alkylated polysiloxane were prepared in two steps by sol-gel spin-coating of flat polymethylhydrosiloxane (PMHS) film of thickness in a micrometer range, and by subsequent hydrosilylation of 1-hexene and *1H, 1H, 2H, 3H, 3H*-tridecafluorononon-1-ene olefins with SiH groups in PMHS gel in quasi-quantitative yields (Sketches of film preparation are in Figures 1–2). The latter olefin was synthesized in a two-steps process: from the radical addition of $C_6F_{13}I$ onto allyl acetate followed by a diodoacetalization of $C_6F_{13}CH_2CHICH_2OCOCH_3$. In the first step, PMHS thin film was anchored onto substrates by hydrolysis of alkoxide precursors, methyldiethoxysilane and triethoxysilane as the crosslinker. They underwent polycondensation reactions in acidic

conditions according to the sol-gel preparation scheme (Scheme 1: step 1). In a second step, the Si–H groups in the H-PMHS film network of 0.8 µm-thick were functionalized in quantitative yield (Figures 1–2) and swollen *via* the well-known hydrosilylation reaction (Scheme 1: step 2).

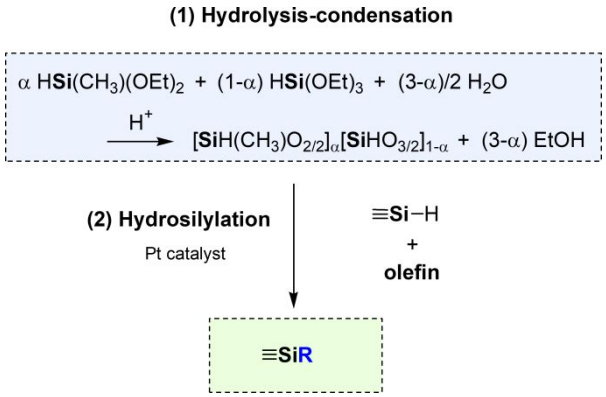


**Scheme 1.** Chemical synthesis of grafted silicon-polymer R-PMHS in two steps: (1) Hydrolysis-condensation reactions in sol-gel process of methyldiethoxysilane and triethoxysilane precursors and (2) hydrosilylation of hydrocarbon or fluorinated olefins with Si-H bonds using Platinum catalyst.

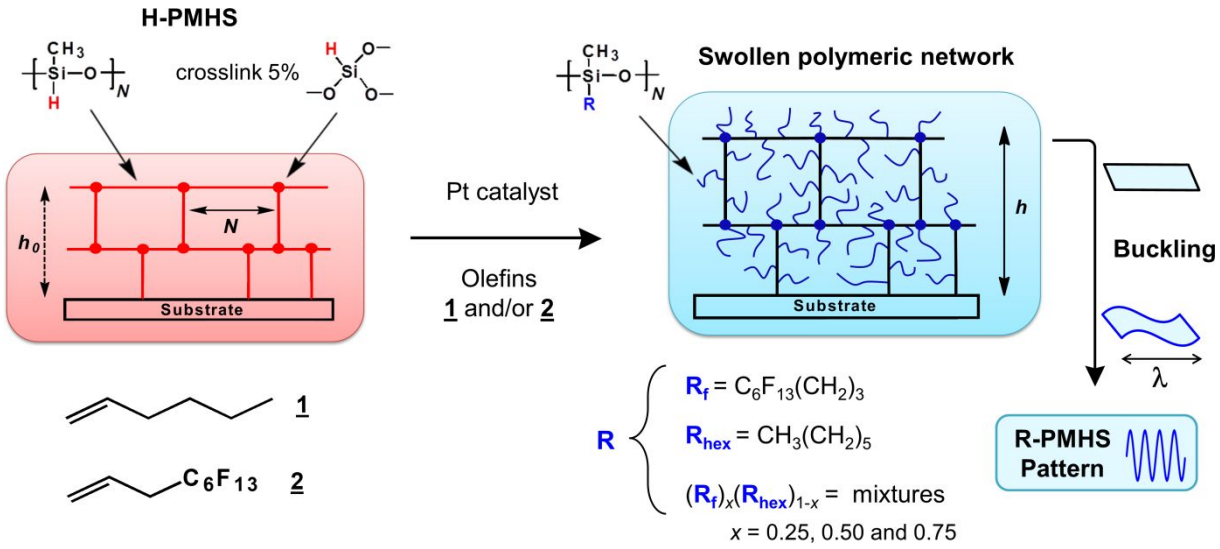


**Figure 1**. Preparation of patterned silicon-polymer surface R-PMHS using hydrosilylation grafting. Schematic representation of anchored elastomeric H-PMHS gel (Red line) and its functionalization *via* hydrosilylation of alkenes bearing alkyl side chains (Blue line) with SiH

groups into grafted R-PMHS catalyzed by Karstedt Pt complex. Chemical structures of olefins (**1**) 1-hexene and (**2**) 1*H*, 1*H*, 2*H*, 3*H*, 3*H*-tridecafluorononon-1-ene. The 3D network is characterized by the average *N* number of repeat units per PMHS segment between trifunctional $SiO_{3/2}$ crosslinks. The irreversible swollen structure of R-PMHS network is depicted by a volume change normal to the surface since the bottom of the polymer film is constrained on the substrate. (λ): Characteristic wavelength of the pattern.

The surface modification and swelling of samples containing fluoroalkyl and hexyl side chains of molecular formulae, $R_{hex}$ = $CH_3(CH_2)_5$- and $R_f$ = $CF_3(CF_2)_5(CH_2)_3$- were characterized by SEM and IR spectroscopy (Figures 2–3). The hexyl side chains in thin film are in a disordered state as evidenced by IR spectroscopy in a previous work.[64] For the fluorinated side chains $CF_3(CH_2)_n(CH_2)_2$- ($n$ = 5), the molecular aggregation occured in bulk polymers or films when $n \geq 7$[80–82] which finally excludes the presence of any crystallized structure in the present study.

### *3.1.2. Synthesis of Crosslinked H-PMHS Films*

In this study, a crosslinker ratio (1-$\alpha$) of 0.05 was chosen to prepare soft elastomeric network denoted H-PMHS.[68] This favors in turn diffusion and subsequent reaction of alkenes molecules, and swelling of thin films.[64] Because of the higher reactivity of SiH substituted precursors toward hydrolytic polycondensation in sol–gel process, they usually yield higher degree of condensation of polysiloxane species[83] in contrast to precursors substituted with bulky organic groups.[84] A schematic representation of the fully crosslinked 3D network is given in Figure 1, neglecting the cycle formation. The chosen substrates were Si100 wafers (A) of Young's modulus 130 GPa[85] and PDMS-based elastomer (B). Substrate B was prepared from elastomer kit Med-4750, resulting in a Young's modulus of 2.2 ± 0.4 MPa

(Figure S1 in Supporting Information). The resulting clear sol was deposited using a spin-coating process forming very flat thin films of same thickness on both substrates ($h_0$ = 0.8 μm) with a good homogeneity as evidenced by SEM cross-sectional images (Figure 3: R = H).

### *3.1.3. Thickness of H-PMHS Films from IR Absorbance*

The thicknesses of spin-coated H-PMHS film, $h_0$, were also measured accurately onto Si wafer substrate A from the intense SiH stretching band $\nu_{SiH}$ at 2169 $cm^{-1}$ (Figure 3A). The peak intensity was calibrated in transmission mode using ellipsometry and their average thickness was found *ca.* 0.8 μm (SD ± 3%; see Supporting Information), assuming the IR absorbance $\nu_{SiH}$ follows eq. S1 similar to that of Beer–Lambert law.[76] This thickness value was confirmed by SEM on both substrates ($h_0 \approx 0.8$ μm). The thickness $h_0$ on substrate B was found to be equal from corrected absorbance of $\nu_{SiH}$ in ATR-FTIR spectra (Figure 3B). This approach enables fast and simple evaluation of $h_0$ on substrate B because its value was below the probed depth of ATR technique (eq. S2) in the order of a few microns. The spectra display also the typical SiH bending band at 839 and 890 $cm^{-1}$ attributed to $SiH(CH_3)O_{2/2}$ subunits in polysiloxane segment[68] (Table S2 and Figure S4).

### *3.1.4. Topography and Nanomechanical Properties of Flat H-PMHS Films*

The topography and nanomechanical properties of the H-PMHS film were determined by PF-QNM microscopy (Figure S2). The height images indicate that both substrates were covered by a dense film which is confirmed by their low roughness of 2.5 nm and 2.9 nm, respectively, on A and B substrates and by homogenous elastic modulus. The Young's moduli were 3.7 ± 0.2 MPa (for A) and 4.8 ± 0.7 MPa (for B) which were in the rubber range in agreement with the average molar mass between crosslinks for the anchored polymer (See calculation from eq. S3 in Supporting Information). Varying the crosslinker ratio from (1-

$\alpha$) = 0.01 to 0.50 induces strong effects with respect to surface mechanichal properties.[68] By contrast, the small increases of both roughness and modulus observed for substrate B as compared to A may be attributed to slight variations of the degree of crosslinking near the surface. One advantage of the sol–gel process is that both the crosslinking and surface attachment can be simultaneously performed to anchor the final thin-film by covalent SiOSi linkages with surface Si-OH groups.[26,27] The surface density of SiOH on the native silicon oxide layer of Si wafer for substrate A was increased after UV-ozone treatment (See Supporting Information). The silicone MED-4750 network (B) is a well-known Pt-cured elastomer by hydrosilylation of vinyl with SiH groups.[86] The near surface chemistry of the silicon network formed *via* hydrosilylation can also produce surface Si-OH groups by auto-oxidation of Si-H.[87] This ultimately leads in sol-gel process to SiOSi linkage with H-PMHS film by co-condensation catalyzed by triflic acid.[73]

### *3.1.5. Preparation of R-PMHS Films by Hydrosilylation of Alkenes*

The hydrosilylation of alkene gives high yields under mild conditions by using transition-metal catalyst mainly based on platinum complexes.[88–90] For the first time, the hydrosilylation of a fluorinated precursor with a crosslinked H-PMHS gel films was achieved to obtain low surface energy materials. The reactivity of the fluorinated precursor toward SiH groups is enhanced using a $CH_2$ spacer between the perfluorinated chain and the reactive double bond.[17,70,91] Thus, reactions with *1H, 1H, 2H, 3H, 3H*-tridecafluorononon-1-ene bearing an allyl group were performed in H-PMHS thin films by immersion in alkene solution (3.3 % v:v) in presence of Karstedt catalyst.[92] Achieved in air at 65 °C in only a few dozen of minutes, the method gave quantitative yields (Figure 2) as evidenced by the vanishing of $\nu_{SiH}$ stretching band of H-PMHS at 2169 $cm^{-1}$ (Figures 3A and 3B) on both substrates, well-monitored by IR.

The absence of $\nu_{SiH}$ band from ATR spectra (Figure 3B), for R-PMHS film thinner than about one micron, clearly indicates that the reactions on substrate B also occurred totally in the bulk of H-PMHS film by diffusion of reagents. At the same time and as expected, the specific CF bands of fluoroalkyl chain $R_f$ appeared at 1240, 1207, 1191 and 1144 $cm^{-1}$.

When the sample was immersed in acetonitrile solution (Figure 2), which is a very poor swelling solvent for silicone, the olefins subsequently diffuse into the bulk of layer because of their hydrophobic nature. The diffusion is also driven by gradient of concentration. The reaction stopped when total loss of SiH species occurred in the bulk polymer film or when swelling of the polymer is limited by the degree of crosslinking. Harnessing networked polymer reactions with olefins (**1**) and (**2**) (Figure 1) gives successful chemical modifications in thin films with organic functional groups $R_f$ and $R_{hex}$. This was confirmed using X-ray Photoelectron Spectroscopy (XPS), Energy Dispersive X-ray (EDX) and FTIR spectroscopy (for a detailed description, see Tables S1– S6, Figures S3 – S8 and related discussion in the Supporting Information). These reactions were also achieved with quasi-full yield in toluene and cyclohexane, based on the disappearance of $\nu_{SiH}$ band at 2169 $cm^{-1}$ (Figure 3) giving rise to grafted polysiloxanes with similar IR features on Si wafer substrate A.

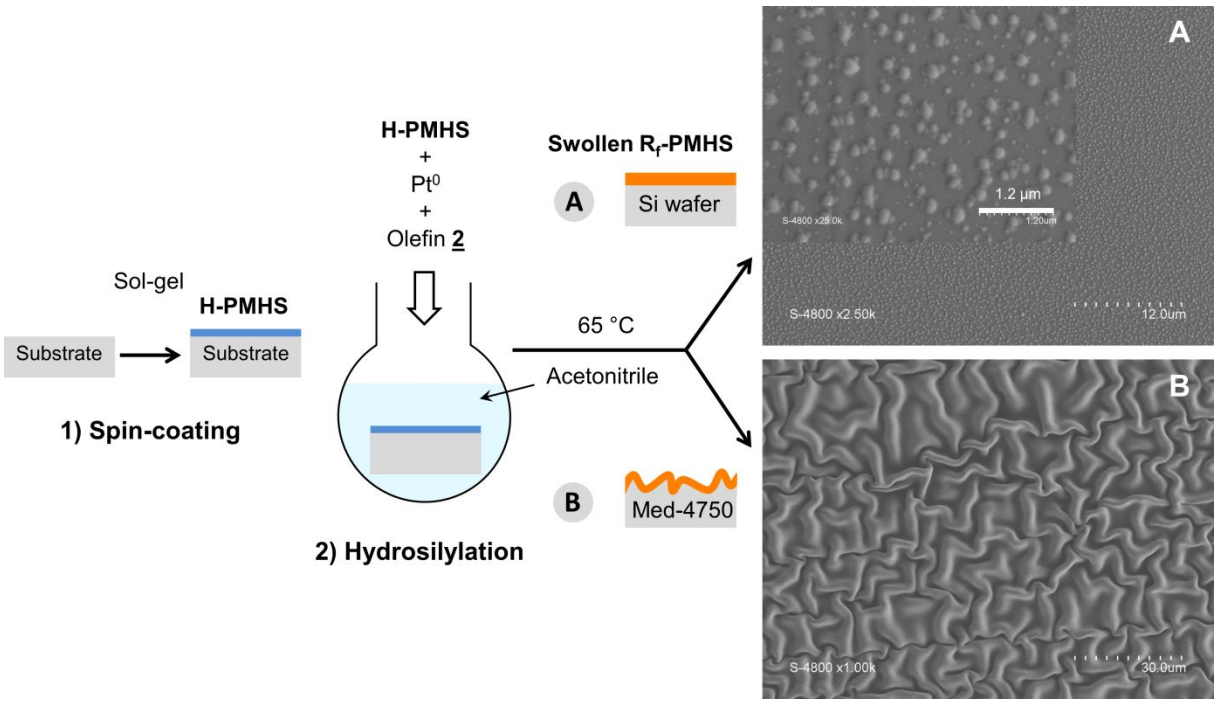


**Figure 2**. Typical micro patterns in swollen fluoroalkyl $R_f$-PMHS film resulting from hydrosilylation of fluorinated olefin **2** by a flat anchored H-PMHS thin film. (A) Dot-like pattern developed on rigid Si wafer substrate A (Insert: 10× magnification image) and (B) Wrinkled pattern developed on soft Med-4750 substrate B. Schematic sample preparation with SiH grafting of alkyl chain and buckling process.

### 3.2. Characteristics of Micro-patterned Surface

The following section presents the effects of reaction on surface morphology and patterns formation performed by using acetonitrile as the solvent to overcome the swelling issues of elastomeric silicone substrate B. The initially flat spin-coated H-PMHS thin film can be attached either on rigid A or soft B substrates. After reaction and swelling, no delamination or cracks were observed, confirming the robustness of the surface attachment.

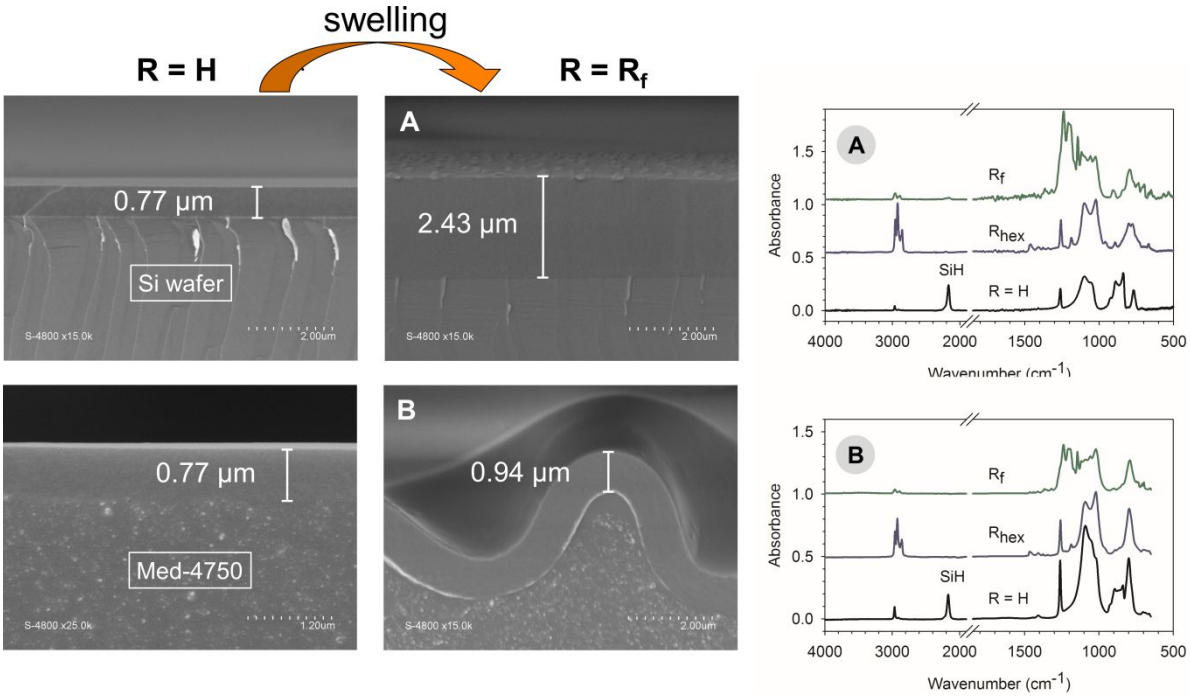


**Figure 3**. Typical SEM cross-sectional view images of micrometric films and thickness measurement: Blank H-PMHS films (R = H) and swollen $R_f$-PMHS films (R = $R_f$) grafted with fluoroalkyl side chain using two distinct substrates A (silicium wafer) and B (silicone elastomer Med-4750). (A) Dot-like and (B) wrinkled patterns resulting from swelling of H-PMHS anchored on various substrates. IR spectra of pristine H-PMHS thin film ($h_0$ = 0.8 µm), and R-PMHS bearing $R_{hex}$ and $R_f$ chains after functionalization *via* catalytic hydrosilylation (same sample) of the corresponding alkenes. (A) IR spectra in transmission mode for films anchored on Si wafer and (B) in ATR mode for films anchored on silicone Med-4750. The total conversion of SiH groups of starting H-PMHS film is shown by the vanishing of SiH band at 2169 $cm^{-1}$.

### *3.2.1. Stability of Micro-patterned Surface*

The PF-QNM, IR and XPS results of $R_{hex}$- and $R_f$-functionalized R-PMHS films on both substrates A and B qualitatively attest to the very good chemical stability of the film after solvent washing with toluene and cyclohexane, even for samples prepared on silicone substrate B, and long term robustness of the alkyl-polysiloxane films. In the latter case (B),

high roughness and opacity (Figure S9) were obtained originated from micro-wrinkling of the top layer. All samples presented in the following were rinsed after reaction with acetonitrile and dried. It is worth noting that the patterns obtained by irreversible swelling of the functionalized samples are "freezing" and do not evolve under ambient condition with time for several months - even years, as monitored by PF-QNM.

### *3.2.2. Young's Modulus of Micro-patterned Surface*

To better understand the effect of surface properties of our system on the pattern formation, PF-QNM microscopy was used to characterize both the topography (Figure 4, height images) and mechanical properties (Figure S10, elastic modulus images) of the swollen R-PMHS films after reactions. The aim was to determine the mismatch mechanical Young's modulus ratio $E_{top}/E_{subs}$ of the top film which is a key factor to the generation of wrinkled patterns. As the precise tip radius may change during scanning the surface due to friction, the Young's modulus was estimated quantitatively before each experiment by calibration, using reference PDMS materials of known elastic modulus (Experimental Part). A comparative study of polysiloxane film stiffness bearing various side groups (R = $R_{hex}$ and $R_f$) on both A and B substrates was attempted with the same tip. The modulus of films was thus measured in the region where the convolution effect of the tip with dot or valley/crest structures can be neglected. Otherwise, the top surface displayed variations in the modulus data closely related to the height modulations of patterns (Figure S10). For samples on substrate A, a mask-covered area on the bottom surface was applied to exclude dots-like structure, and the Young's modulus was measured including only masked region. For samples on substrate B, the modulus was measured on large flat and homogeneous region surrounded by ridges of *ca.* 20 µm size (Figure 4). The bar plot presented in Figure 5b indicates that the Young's modulus of R-PMHS films assessed by this method are similar on substrates A and B, as anticipated by using same reaction conditions. However, the Young's modulus of the top films increases as

expected with the molar mass of substituent R grafted onto siloxane units from $R_{hex}$ to $R_f$. Therefore, we anticipated that the wavelength of patterns (λ) of $R_f$-film would be larger than that of $R_{hex}$-film (*Vide infra*).

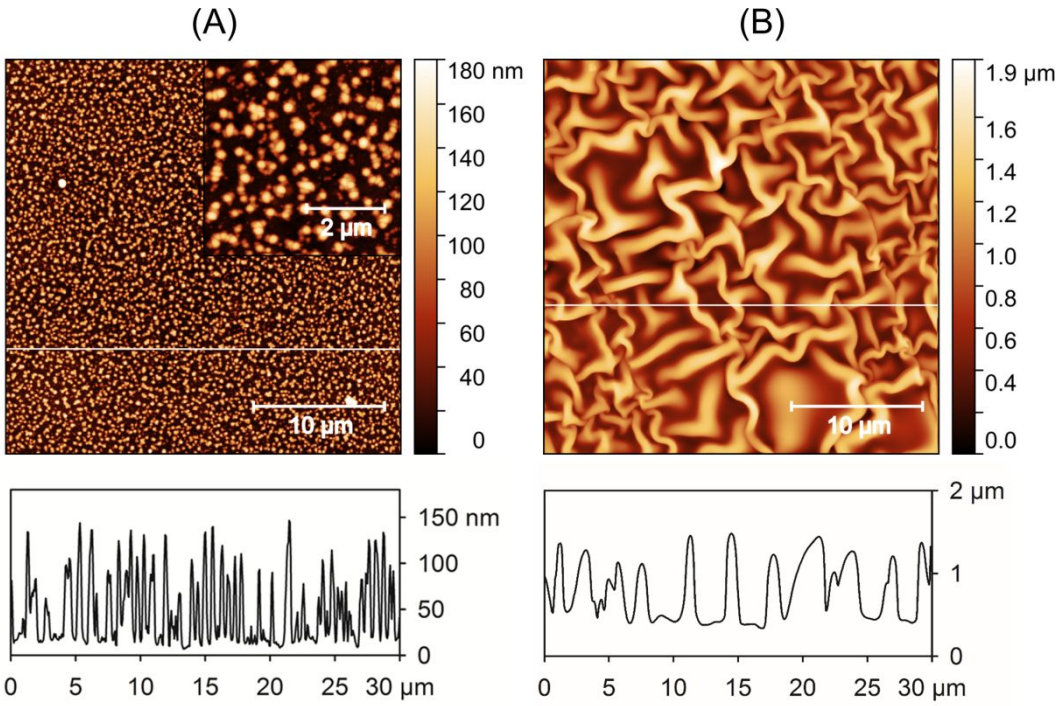


**Figure 4**. Representative maps of topography of 30 × 30 µm$^2$ region in PeakForce QNM mode of random and inhomogeneous micro patterns generated by swelling and hydrosilylation of 1*H*, 1*H*, 2*H*, 3*H*, 3*H*-tridecafluorononon-1-ene (**2**) with H-PMHS, giving fluorinated films $R_f$-PMHS. (A) Dot-like pattern of wavelength λ = 0.4–0.7 µm on rigid Si wafer substrate A with map inserts of 5 × 5 µm$^2$ region and (B) Wrinkled patterns of λ = 4–7 µm on soft elastomeric substrate B. Profile section analysis according to the white lines shown in height images.

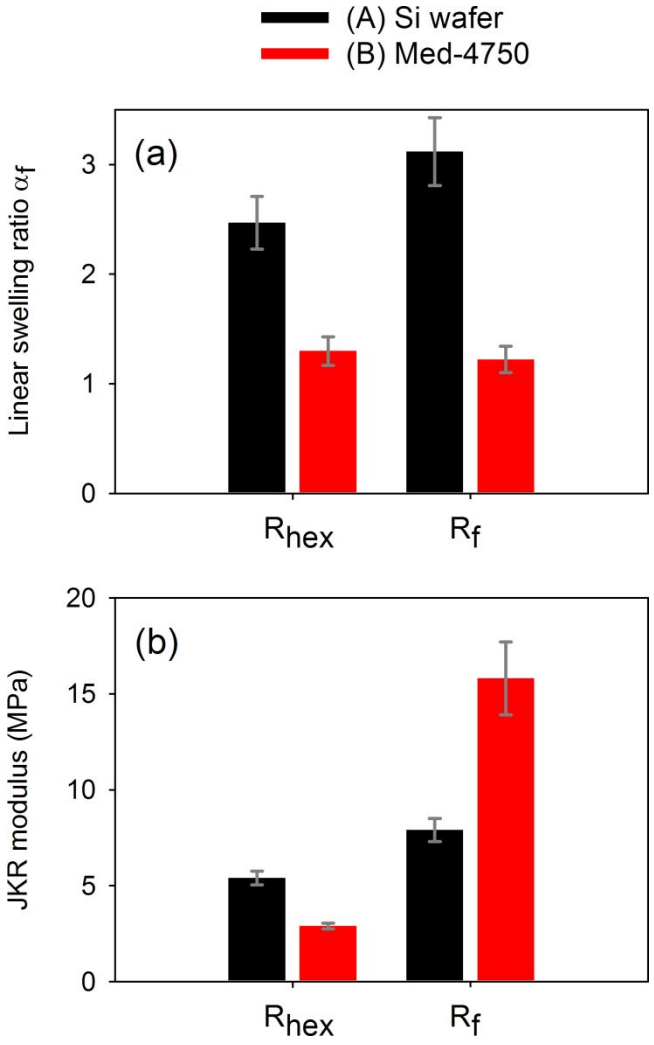


**Figure 5**. Swelling expansion ratio ($\alpha_f$) in the swollen state and mechanical properties of modified R-PMHS (R = $R_f$ or $R_{hex}$) top films anchored onto rigid Si wafer A and elastomeric B substrates. (a) Swelling ratio $\alpha_f = h/h_0$ (eq. 1) of the top films measured from SEM thickness ($h$) of alkyl R-PMHS and ($h_0$) of the starting H-PMHS film. (b) JKR modulus determined from PF-QNM mapping.

### *3.2.3. Swelling of R-PMHS Layer*

The driving force for the creation of micro-pattern of wrinkling originated from the swelling of side chains. Therefore, a variety of wrinkle morphologies was observed by different microscopy techniques (Figures 2–4) such as dots, folds or wrinkles which are related with geometry of the systems and the level of compressive stress developed within the gel by

swelling. The SEM and PF-QNM observations (Figures 2–4) showed that two different inhomogeneous random patterns are formed by swelling: dot-like pattern on substrate A with spots of high aspect ratios and space-out of 0.4–0.7 μm as measured between the spots, and micro-wrinkled pattern on substrate B with wavelength of 4–7 μm between the ridges. Moreover, the observed random patterns are also characterized by different amplitudes of undulation ($A$) in the micrometer range, as shown by profiles section (Figure 4). To explain the differences experienced in same reaction conditions by swelling of top film of initial thickness ($h_o$ = 0.8 μm), two distinct physical approaches for wrinkles formation must be considered.[35] In the first case, the system consists of a uniform swelling gel layer bound to a rigid silicon wafer substrate (A).[42] In the second one, also known as the bilayer system,[56] the layer is made by a stiff swelling gel layer linked to a soft non-swelling elastomer foundation Med-4750 (B). Using both approaches, we will thus discuss the effect of swelling ratios on the transition of flat H-PMHS film of thickness, $h_o$, to micro-structured swollen final R-PMHS film of thickness, $h$. The swelling ratio after reaction can be simply defined by the expansion of the film thickness ($\alpha_f$), according to eq. (1) which is commonly used to determine the onset of surface instability in constrained hydrogel systems:[41,43,45,48]

$$\alpha_f = \frac{h}{h_0} \qquad (1)$$

where $h$ and $h_0$ were determined by SEM measurement (Figure 3). In the case of constrained film on rigid substrate A, $\alpha_f$ is approximately equal to the volumetric swelling ratio because the thin film swells essentially in the direction perpendicular to the substrate.

In our systems, the patterns are self-generated through swelling by reaction of SiH groups in the H-PMHS matrix. In all cases, the surface structuration of the thin films, as previously

prepared (Figure 3), was characterized in the swollen state after total conversion of SiH into $R_{hex}$ or $R_f$ side-chain.

### *3.2.4. Patterns Formed on Rigid Silicon Wafer Substrate*

The dot-like structure formed on rigid wafer substrate A (Figures 2A, 4A and S17) resembles to hexagonal patterns observed in uniform hydrogel layer constrained on rigid substrate by using water or solvent. The anisotropic expansion of the surface-attached polymer gel perpendicular to the surface generates compressive stress (σ) within the gel. These mechanical stresses can be described as the in plane compression induced by the strain $\varepsilon = (L - L_o)/L_o$ for a fictive unconstrained gel of $L_o$ length in the initial dry state and of $L$ length in the swollen state. When the growth-induced mechanical stress exceeds a critical value for buckling ($\sigma > \sigma_c$), there is a sudden change in shape of the top R-PMHS surface to relieve stress resulting in pattern formation (Figure 1). The mechanical instability is usually characterized by a strain mismatch between the top film and the substrate with different elastic Young's moduli ($E_{top}$ and $E_{subs,}$ respectively).

The wavelength (λ) of the pattern can be controlled linearly by changing the thickness ($h$) which are normally in the same order of magnitude ($\lambda \approx h$) but with different prefactors. For a swollen gel constrained on a rigid substrate, a quantitative estimate of the prefactor of the linear relationship between ($\lambda$) and ($h$) is given by eq. 2:[35,42]

$$\frac{\lambda}{h} = \frac{2\pi}{3^{1/2}}\left(\frac{E_{top}}{E_{subs}}\right)^{1/4} \qquad (2)$$

The characteristic wavelength is also dependent on the $E_{top}/E_{subs}$ modulus ratio of the film to the substrate. Using eq. 2, and the $E_{top}$ values measured by PF-QNM for top films $R_{hex}$ (5.2 MPa) and $R_f$ (7.5 MPa), and $E_{subs}$ = 130 GPa for Si100 wafer[85] wavelength values ($\lambda$) of 0.5

and 0.8 µm were calculated, respectively, on the basis of SEM thicknesses $h^{Rhex}$ = 1.9 µm (Figure S11) and $h^{Rf}$ = 2.4 µm (Figure 3A). Despite it was experimentally difficult to observe a significant difference between λ for $R_f$- and $R_{hex}$-patterns (Figures 4A and S12b), the calculated values are in agreement with experimental observations in the 0.4–0.7 µm range estimated from height profiles between the spots. The final topology of the surface can be regarded as "flat" because the gel swells uniformly, and the final amplitude of modulation $A \approx$ 0.1 µm (Figure 4) was low compared to their SEM thickness. As expected, the swelling ratio, $\alpha_f$, is clearly higher for $R_f$-film (3.5) than that for $R_{hex}$-film (2.5) (Figure 5a, bar plot A) due to the higher bulkiness of $R_f$ radical. A swelling ratio difference is noted between wafer substrate (A) and silicone Med-4750 (B) in Figure 5a. However, for reactions achieved in the same conditions, it can be anticipated that the volumetric swelling ratio of the network is the same for both substrates. This explains why the unidirectional swelling ratios ($\alpha_f$) measured with eq. 1 decreases from 2.5–3.1 (A) to ≈ 1.25 (B) (Figure 5a), because in the situation (B) (Section 3.2.5), the network swells also in 2D plane with wrinkles of high amplitude $A \approx 1$ µm (Figures 4B and 6).

The high $\alpha_f$ values measured from 2.5 to 3.5 with our systems are above the critical threshold value reported for various hydrogel systems of $\alpha_c \approx 2$ for the polyacrylamide,[43] $\alpha_c \approx 1.12$ for the PHEMA[45] and $\alpha_c \approx 2$ for the poly(vinyl pyrrolidone)/poly(acrylic acid)[49] layer-by-layer system. In fact, there is a wide range of critical swelling values on the onset of surface instability reported experimentally, 2.0–3.7 in hydrogel material,[46] or theoretical prediction from 2.5 to 3.4.[48] In this present work, the high swelling ratios indicate that surface buckling occurred easily upon swelling. The typical dot-like shape pattern can be easily obtained with a $R_{hex}$:$R_f$ mixture prepared in the same conditions (Figures S11–S12a). Previous works[66,67] have also reported that blank H-PMHS film swollen by reaction in toluene with hydrophilic

phospholipid precursors gave creasing pattern with sharp folds (Figure S13) similar to those observed in elastomer films[57] and in hydrogel systems.[41,43] It can be highlighted here that these surface patterns, originated likely from swelling of H-PMHS film constrained on rigid substrate, show that the method is universal.

### *3.2.5. Wrinkled Patterns Formed on Soft Silicone Elastomer*

The top film prepared on silicone elastomer (B) produces inhomogeneous random wrinkles (Figures 2–4) upon swelling forming a maze-like surface pattern consisting in zig-zag for valleys and ridges. Our system looks like wrinkle morphologies of swollen rigid oxide thin film in presence of solvent on surface-oxidized PDMS[38,50,51] or polystyrene[53] soft substrates with UV-Ozone technique. The optical (Figure S14) and PF-QNM (Figure 4B) images evidenced the presence of large flat regions surrounded by ridges, around 20 μm in size, where there is no apparent buckling. It must be emphasized that different coexisting kinetically trapped morphologies[38] were also observed from top view image (Figures 4B and S14) resulting in a rapid kinetic of swelling. Moreover, the observed topography of cross-sectional view of the film after reaction (Figure 6) shows different shapes in the form of smooth micro-scale wrinkles together with local sharp fold. These observations indicate that local mechanical stresses may vary in magnitude across the surface of the sample.

In the case of soft substrate B, the well-known system of equations for the bilayer model of a swollen stiff top film bound to a soft non-swelling elastomer foundation can be applied similarly, according to classical theory (eqs. 3–5):[38,52,55,56]

$$\frac{\lambda}{h} = \frac{2\pi}{3^{1/3}}\left(\frac{E_{top}}{E_{subs}}\right)^{1/3} \qquad (3)$$

$$\varepsilon_c = \frac{3^{2/3}}{4}\left(\frac{E_{subs}}{E_{top}}\right)^{2/3} \quad (4)$$

$$\frac{A}{h} = \sqrt{\frac{\varepsilon}{\varepsilon_c} - 1} \quad (5)$$

where ($\varepsilon_c$) stands for the compressive critical strain for buckling to occur and (ε) for the applied strain by swelling. Using eq. (3) and the measured parameters, $E_{top}$ for $R_{hex}$-film (2.4 MPa) and $R_f$-film (16 MPa), and $E_{subs}$ = 2.2 MPa for the elastomeric foundation (B), wavelength values λ of 4.5 and 7.9 μm were respectively calculated, on the basis of SEM thicknesses for $h^{Rhex}$ = 1.0 μm (Figure S11) and $h^{Rf}$ = 0.94 μm (Figure 3B), in agreement with experimentally measured values of 4–5 μm and 5–7 μm, respectively. The critical strain ($\varepsilon_c$) calculated from eq. 4 was only 14% for $R_f$-film and 50% for $R_{hex}$-film. This means that the $R_f$-film of higher skin stiffness initially forms wrinkles at a lower compressive strain than the $R_{hex}$-film does. In contrast to case A (Section 3.2.4), the values of linear swelling ratios $\alpha_f$ (in the direction perpendicular to the film) are close between $R_{hex}$- and $R_f$-wrinkled surfaces (Figure 5a, bar graph A). However, in the particular case of a wrinkled film, the specific in plane swelling of films could be larger for $R_f$-film than for $R_{hex}$-film due to the higher bulkiness of the $R_f$-grafted fluorinated chain. If the difference in swelling ratio between $R_{hex}$ and $R_f$ components on substrate B (Figure 5a, bar graph B) is neglected, the higher stiffness of fluorinated $R_f$-film could thus explain the different wrinkle density observed between $R_{hex}$- and $R_f$-films (Figures 4B, S12d and S14). Indeed, the $R_{hex}$-surface displays larger proportion of flat region without wrinkles than the $R_f$ surface. The room temperature reaction of 1-hexene gave similar structure and wrinkle density from SEM and optical microscopies (Figure S15) because the thermal expansion coefficient of silicone rubber is negligible compared to the strain (ε) induced by the swelling of the H-PMHS layer. The proposed method can be

extended straightforward to $R_{hex}$:$R_f$ mixtures of olefins (Figures S11 and S12c) and a hydrophilic precursor allyl triethylene glycol monomethyl ether (Figure S16). As observed in Figures S11, S12c and S16, the surfaces in the swollen state reveal the formation of various patterns from wrinkles to creases in thin films. This illustrates the concept of buckling by hydrosilylilation of olefins with constrained H-PMHS network is a general approach to be employed for the creation of long-term microstructures with various functions.

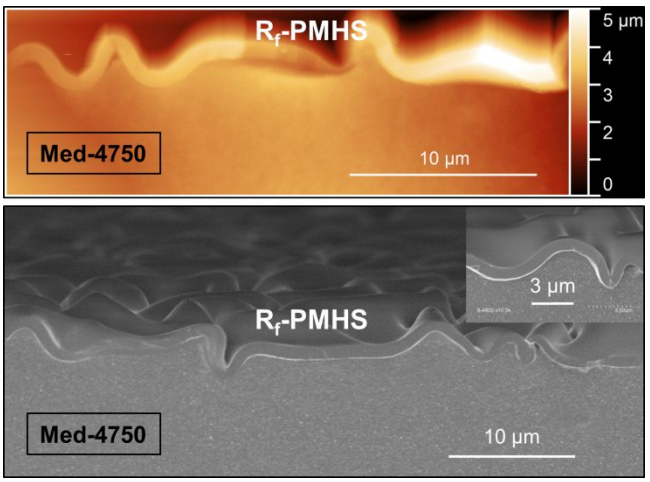


**Figure 6.** Typical wrinkled structures due to swelling showing formation of micro-scale smooth ripples and a local sharp fold instability (insert SEM image). (Up) Atomic force microscopy and (Bottom) SEM cross-sectional view images of fluoroalkyl $R_f$-PMHS film prepared on silicone elastomer Med-4750 (B).

### 3.3. Wetting Properties of the Patterned Surface

The measurements of water contact angle (WCA), ethylene glycol contact angle (ECA) and *n*-hexadecane contact angle (HCA) were performed to assess the hydrophobicity of functionalized polysiloxane surface $R_f$-PMHS or $R_{hex}$-PMHS (Figures 7-8 and Table 1). As expected, the water contact angle (WCA) hysteresis of fluorinated chain ($R_f$) was enhanced upon roughening the surfaces giving highly hydrophobic surface properties for water with static/hysteresis WCA of 136°/74° in the resulting wrinkle pattern (B). These values are

higher than that of 119°/41° measured on the smoother "flat" dot-like patterned surface formed on Si wafer A (Figure 7). Moreover, the WCA hysteresis, $\theta_{hys}$, obviously decreased from 74° to 41° with decreasing of surface roughness (Figure 4) of two orders of magnitude between wrinkles and dots-like patterns. The surface performance of our system may be further optimized according to the thickness and degree of crosslinking of the H-PMHS thin film in order to increase the amplitude of the wrinkled surfaces.

The solid surface energy ($\gamma_S$) was calculated from the WCA, ECA and HCA values by using the Owens and Wendt's method [79] on films anchored on Si wafer (A). The surface tension decreases in the order of $–CH_2– > –CH_3 > –CF_2– > –CF_3$.[93] Thus, the polysiloxane bearing fluoroalkyl chains obviously displayed lower surface energy than that of polysiloxane grafted with hexyl chains (Figure 8). The surface of fluorinated alkyl chain $R_f$-PMHS displays an extremely low surface energy value of 15 mN/m. This result is expected for polymer having high surface density of $–CF_2$ and $–CF_3$ groups, together with high ratio of $–CF_3$ groups with respect to $–CF_2$ groups, as reported for pendant fluorosilicone.[17,94] While in comparison, the surface energy of $–CF_2$- such as Teflon® is 18.5 mN/m.[94] The presence of $\underline{C}F_3$ and $\underline{C}F_2$ components at the surface were confirmed from high resolution C1s XPS spectrum (Figures S7 and S8) by a C1s peak ratio of 5 (Table S3) in good agreement with the perfluorohexyl structure.[95]

Tuning the hydrophobic properties of R-PMHS surface anchored on Si wafer (A) by hydrosilylation of mixtures of alkenes (**1**) and (**2**) was further investigated. Figure 8 shows that the XPS fluorine F1s % content near the surface correlated well with contact angles *versus* the x molar ratio of alkyl side chains. The WCA or ECA curves and particularly HCA steadily increase *versus x,* in agreement with F1s % curve.

29

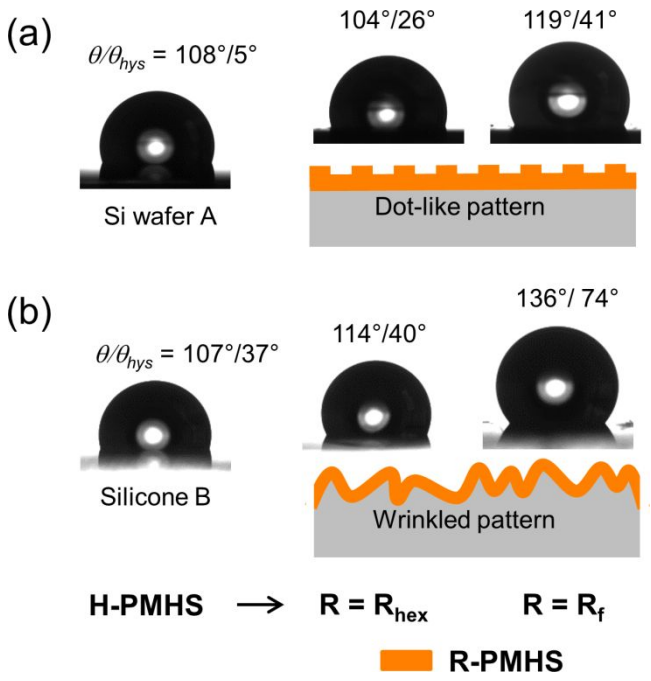


**Figure 7.** Static/hysteresis ($\theta/\theta_{hys}$) water contact angles of different R-PMHS micro patterns (R = $R_{hex}$ and $R_f$) formed upon swelling of hydrophobic films (right), and of pristine H-PMHS flat film (left). (a) Sample films anchored on rigid Si wafer (A) generating dot-like pattern. (b) Sample films anchored on silicone elastomer Med-4750 (B) generating wrinkled pattern. $\theta_{hys}$ is the difference between the advancing contact angle $\theta_{adv}$ and receding contact angles $\theta_{rec}$ as summarized in Table 1.

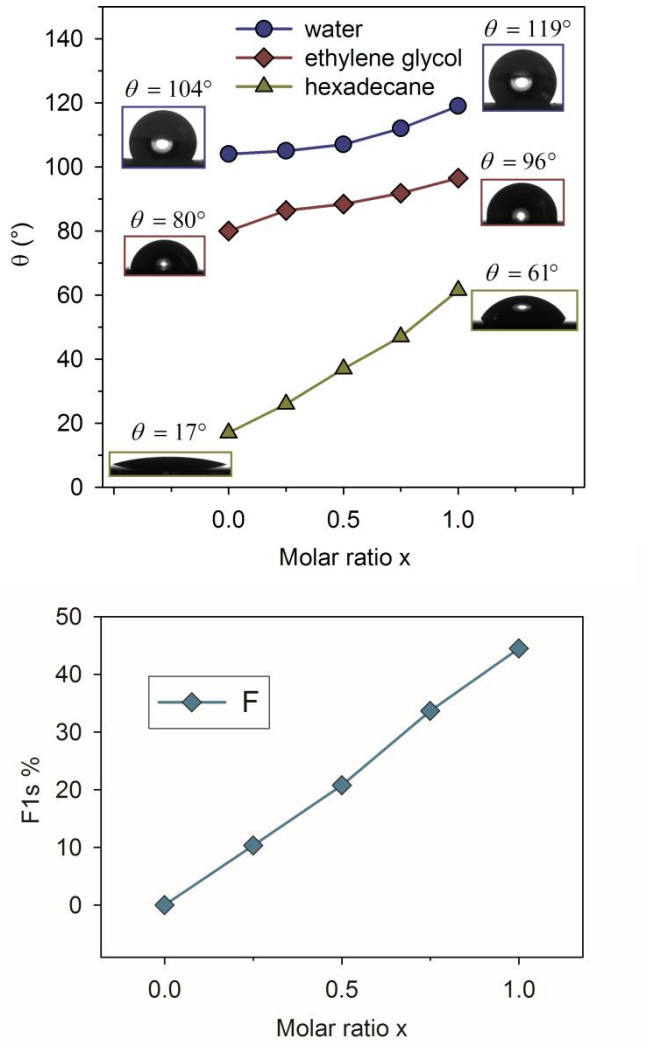


**Figure 8.** Tunable hydrophobicity (top) and F1s composition (bottom) *versus* the molar ratio of alkenes ($x$) = $[R_f]_0/([R_f]_0+[R_{hex}]_0)$, where $[R_f]_0$ and $[R_{hex}]_0$ stand for the concentrations of $C_6F_{13}CH_2CH{=}CH_2$ at $t$ = 0 and $C_3H_7CH_2CH{=}CH_2$ at $t$ = 0, respectively, for alkylated $(R_f)_x(R_{hex})_{1-x}$-PMHS flat surfaces, prepared on Si wafer substrate (A). (Up) Contact angles evolution for films *versus* the molar ratio of alkene mixtures ($x$) with droplets of water, ethylene glycol and *n*-hexadecane having liquid surface tension ($\gamma_L$) of 72.8, 48.0 and 27.5 mN/m, respectively. The surface energy for homogenous alkyl surfaces $R_{hex}$- and $R_f$-PMHS was calculated from the contact angles of the three probing liquids using the Owens and Wendt's method:[79] $\gamma_S$ ($R_{hex}$) = 25.6 mN/m and $\gamma_S$ ($R_f$) = 15.0 mN/m (See Tables S7 and S8 and Figure S18 in the ESI). (Bottom) Evolution of the fluorine F1s composition (atomic

%) F1s at 689.1–688.7 eV *versus* (*x*) for the corresponding functionalized surfaces by using mixture of hexyl ($R_{hex}$) and fluoroalkyl chains ($R_f$) (See ESI).

**Table 1.** Static water contact angles (deg) and dynamic water contact angles (deg) of anchored H-PMHS films (thickness $h_0$= 0.8 μm) and alkylated R-PMHS films (R = $R_{hex}$ and $R_f$) on substrates (A) Si wafer and (B) silicone Med-4750.

| Substrates | R-PMHS films | $\theta$ (°) | $\theta_{adv}$ | $\theta_{rec}$ |
|---|---|---|---|---|
| (A) Si wafer | H-PMHS | 108 | 109 | 104 |
| (A) Si wafer | $R_{hex}$-PMHS | 104 | 107 | 81 |
| (A) Si wafer | $R_f$-PMHS | 119 | 120 | 79 |
| (B) Med-4750 | H-PMHS | 107 | 108 | 71 |
| (B) Med-4750 | $R_{hex}$-PMHS | 114 | 120 | 80 |
| (B) Med-4750 | $R_f$-PMHS | 136 | 142 | 68 |

$\theta$, $\theta_{adv}$, and $\theta_{rec}$ are static contact angle, advancing contact angle and receding contact angle, respectively (Standard deviations: $\theta$ ± 1 deg, $\theta_{adv}$ and $\theta_{rec}$ ± 2 deg).

## 4. Conclusion

Soft polymethylhydrosiloxane (PMHS) coatings have been crosslinked and anchored *via* sol-gel copolymerization of mixture of hydrogenosilane precursors, methyldiethoxysilane and triethoxysilane as crosslinker, on both oxidized rigid silicon wafer and soft silicone model substrates. The crosslinked H-PMHS film was subsequently swollen by quantitative hydrosilylation of hydrocarbon and fluorinated olefins within the polymer network inducing the formation of permanent wrinkled surfaces in the swollen state. This approach provides a simple and general method to produce long-term pattern surfaces with a variety of functions. The chemical structure of the polymer functionalized with hexyl or fluoroalkyl groups affected both the wrinkled characteristics and wetting properties as well as Young's moduli of

the top surfaces. After reaction of flat pristine H-PMHS, the surface topography revealed the presence of inhomogeneous wrinkled micropatterns on the soft silicone elastomeric surface. The differences in pattern formation on both substrates were explained by swelling after reaction using classical theory for buckling. The wavelengths of the different patterns were thus predicted in good agreement with the observed values. The functional PMHS coatings open a new route for the engineering of hydrophobic solid surfaces. The spontaneous formation of wrinkle patterns onto swollen PMHS is a general approach which may be useful to design robust and permanent wrinkled structures on soft material such as PDMS. This method allowed the achievement of a variety of functional specific devices with finely tuned surface energy such as medical implants, catheters, vessels or small reservoirs for biomedical items and in microfluidics. This approach was also extended to hydrophilic precursors for biomedical applications, under progress.

**Supporting Information**

Additional experimental details (thin film preparation, film thicknesses and calculation of surface energies) and wrinkled films, methods, IR (transmission and ATR, including calibration curves of absorbance ratios) and XPS spectra, EDX data, film wetting data and related discussions, PF-QNM and SEM images of blank PMHS film and wrinkled structures in swollen R-PMHS films, including optical microscope images (PDF). The Supporting Information is available free of charge at https://pubs.acs.org/doi/

**Acknowledgements**

This work was supported in part by Sanofi and AVIESAN under project SAMI (Coord. Elisabeth Delevoye at CEA-LETI Grenoble). We thank Atofina (Pierre Bénite, France) for

supplying $C_6F_{13}I$, Dr Gérald Lopez for the preparation of allyl-$C_6F_{13}$ and CNRS for financial support.

## References

(1) Smith, D.; Iacono, S.; Iyer, S. S. *Handbook of Fluoropolymer Science and Technology*; Wiley, New York, 2014. https://doi.org/10.1002/9781118850220.

(2) Ameduri, B.; Fomin, S. *Fascinating Fluoropolymers and Their Applications - 1st Edition*, Elsevier.; Oxford, 2020.

(3) Archer, R. J.; Becher-Nienhaus, B.; Dunderdale, G. J.; Hozumi, A. Recent Progress and Future Directions of Multifunctional (Super)Wetting Smooth/Structured Surfaces and Coatings. *Advanced Functional Materials* **2020**, *30* (26), 1907772. https://doi.org/10.1002/adfm.201907772.

(4) Wang, S.; Liu, K.; Yao, X.; Jiang, L. Bioinspired Surfaces with Superwettability: New Insight on Theory, Design, and Applications. *Chem. Rev.* **2015**, *115* (16), 8230–8293. https://doi.org/10.1021/cr400083y.

(5) Nakajima, A.; Hashimoto, K.; Watanabe, T.; Takai, K.; Yamauchi, G.; Fujishima, A. Transparent Superhydrophobic Thin Films with Self-Cleaning Properties. *Langmuir* **2000**, *16* (17), 7044–7047. https://doi.org/10.1021/la000155k.

(6) Zhang, R.; Liu, Y.; He, M.; Su, Y.; Zhao, X.; Elimelech, M.; Jiang, Z. Antifouling Membranes for Sustainable Water Purification: Strategies and Mechanisms. *Chem. Soc. Rev.* **2016**, *45* (21), 5888–5924. https://doi.org/10.1039/C5CS00579E.

(7) Lin, H.; Hu, Q.; Liao, T.; Zhang, X.; Yang, W.; Cai, S. Highly Hydrophobic Cotton Fabrics Modified by Poly(Methylhydrogen)Siloxane and Fluorinated Olefin: Characterization and Applications. *Polymers* **2020**, *12* (4), 833. https://doi.org/10.3390/polym12040833.

(8) Ma, W.; Ameduri, B.; Takahara, A. Molecular Aggregation Structure and Surface Properties of Biomimetic Catechol-Bearing Poly[2-(Perfluorooctyl)Ethyl Acrylate] and Its Application to Superamphiphobic Coatings. *ACS Omega* **2020**, *5* (14), 8169–8180. https://doi.org/10.1021/acsomega.0c00439.

(9) Yang, T.; Choo, J.; Stavrakis, S.; Mello, A. Fluoropolymer Coated PDMS Microfluidic Devices for Application in Organic Synthesis. *Chemistry* **2018**, *24*. https://doi.org/10.1002/chem.201802750.

(10) Riche, C. T.; Zhang, C.; Gupta, M.; Malmstadt, N. Fluoropolymer Surface Coatings to Control Droplets in Microfluidic Devices. *Lab Chip* **2014**, *14* (11), 1834–1841. https://doi.org/10.1039/C4LC00087K.

(11) Guo, Y.; Li, K.; Hou, C.; Li, Y.; Zhang, Q.; Wang, H. Fluoroalkylsilane-Modified Textile-Based Personal Energy Management Device for Multifunctional Wearable Applications. *ACS Appl. Mater. Interfaces* **2016**, *8* (7), 4676–4683. https://doi.org/10.1021/acsami.5b11622.

(12) Meuler, A. J.; Smith, J. D.; Varanasi, K. K.; Mabry, J. M.; McKinley, G. H.; Cohen, R. E. Relationships between Water Wettability and Ice Adhesion. *ACS Appl. Mater. Interfaces* **2010**, *2* (11), 3100–3110. https://doi.org/10.1021/am1006035.

(13) Han, Z.; Feng, X.; Guo, Z.; Niu, S.; Ren, L. Flourishing Bioinspired Antifogging Materials with Superwettability: Progresses and Challenges. *Advanced Materials* **2018**, *30* (13), 1704652. https://doi.org/10.1002/adma.201704652.

(14) Thanawala, S. K.; Chaudhury, M. K. Surface Modification of Silicone Elastomer Using Perfluorinated Ether. *Langmuir* **2000**, *16* (3), 1256–1260. https://doi.org/10.1021/la9906626.

(15) Higaki, Y.; Ishige, R.; Takahara, A. *Fluoropolymer Surfaces/Interfaces*; Smith, D. W., Iacono, S. T., Iyer, S. S., Eds.; Blackwell Science Publ: Oxford, 2014.

(16) Chhatre, S. S.; Guardado, J. O.; Moore, B. M.; Haddad, T. S.; Mabry, J. M.; McKinley, G. H.; Cohen, R. E. Fluoroalkylated Silicon-Containing Surfaces−Estimation of Solid-Surface Energy. *ACS Appl. Mater. Interfaces* **2010**, *2* (12), 3544–3554. https://doi.org/10.1021/am100729j.

(17) Pasquet, C.; Longuet, C.; Hamdani - Devarennes, S.; Ameduri, B.; Ganachaud, F. Comparison of Surface and Bulk Properties of Pendant and Hybrid Fluorosilicones. In *Silicone Surface Science*; M.J. Owen & R. Dvornic: Washington, USA, Chapter 5, 2012; pp 115–178.

(18) Quéré, D. Wetting and Roughness. *Annual Review of Materials Research* **2008**, *38* (1), 71–99. https://doi.org/10.1146/annurev.matsci.38.060407.132434.

(19) Wang, S.; Liu, K.; Yao, X.; Jiang, L. Bioinspired Surfaces with Superwettability: New Insight on Theory, Design, and Applications. *Chem. Rev.* **2015**, *115* (16), 8230–8293. https://doi.org/10.1021/cr400083y.

(20) Golovin, K.; Lee, D. H.; Mabry, J. M.; Tuteja, A. Transparent, Flexible, Superomniphobic Surfaces with Ultra-Low Contact Angle Hysteresis. *Angewandte Chemie International Edition* **2013**, *52* (49), 13007–13011. https://doi.org/10.1002/anie.201307222.

(21) Tuteja, A.; Choi, W.; Mabry, J. M.; McKinley, G. H.; Cohen, R. E. Robust Omniphobic Surfaces. *Proceedings of the National Academy of Sciences* **2008**, *105* (47), 18200–18205. https://doi.org/10.1073/pnas.0804872105.

(22) Tuteja, A.; Choi, W.; Ma, M.; Mabry, J. M.; Mazzella, S. A.; Rutledge, G. C.; McKinley, G. H.; Cohen, R. E. Designing Superoleophobic Surfaces. *Science* **2007**, *318* (5856), 1618–1622. https://doi.org/10.1126/science.1148326.

(23) Kamei, J.; Yabu, H. On-Demand Liquid Transportation Using Bioinspired Omniphobic Lubricated Surfaces Based on Self-Organized Honeycomb and Pincushion Films. *Advanced Functional Materials* **2015**, *25* (27), 4195–4201. https://doi.org/10.1002/adfm.201501020.

(24) Vogel, N.; Belisle, R. A.; Hatton, B.; Wong, T.-S.; Aizenberg, J. Transparency and Damage Tolerance of Patternable Omniphobic Lubricated Surfaces Based on Inverse Colloidal Monolayers. *Nat Commun* **2013**, *4* (1), 1–10. https://doi.org/10.1038/ncomms3176.

(25) Wong, T.-S.; Kang, S. H.; Tang, S. K. Y.; Smythe, E. J.; Hatton, B. D.; Grinthal, A.; Aizenberg, J. Bioinspired Self-Repairing Slippery Surfaces with Pressure-Stable Omniphobicity. *Nature* **2011**, *477* (7365), 443–447. https://doi.org/10.1038/nature10447.

(26) Mittal, K. L. *Silanes and Other Coupling Agents, Volume 5*; CRC Press: London, 2012. https://doi.org/10.1201/b12244.

(27) Pluedemann, E. P. In *Silane Coupling Agents*; Plenum Press: New York, 1982; p 22.

(28) Maciejewski, H.; Karasiewicz, J.; Dutkiewicz, M.; Nowicki, M.; Majchrzycki, Ł. Effect of the Type of Fluorofunctional Organosilicon Compounds and the Method of Their Application onto the Surface on Its Hydrophobic Properties. *RSC Adv.* **2014**, *4* (95), 52668–52675. https://doi.org/10.1039/C4RA07392D.

(29) Jennings, A. R.; Iacono, S. T. Progress in Fluorinated Organically Modified Silicas. *Polymer International* **2016**, *65* (1), 6–10. https://doi.org/10.1002/pi.4984.

(30) Raj, S. S.; Mathew, R. M.; Nair, Y.; Aruna, S. T.; Vinod, T. P. Fabrication and Applications of Wrinkled Soft Substrates: An Overview. *ChemistrySelect* **2022**, *7* (16), e202200714. https://doi.org/10.1002/slct.202200714.

(31) González-Henríquez, C. M.; Rodríguez-Hernández, J. *Wrinkled Polymer Surfaces: Strategies, Methods and Applications*; Springer International Publishing: Cham, 2019. https://doi.org/10.1007/978-3-030-05123-5.

(32) Li, Y.; Dai, S.; John, J.; Carter, K. R. Superhydrophobic Surfaces from Hierarchically Structured Wrinkled Polymers. *ACS Appl. Mater. Interfaces* **2013**, *5* (21), 11066–11073. https://doi.org/10.1021/am403209r.

(33) Zang, J.; Ryu, S.; Pugno, N.; Wang, Q.; Tu, Q.; Buehler, M. J.; Zhao, X. Multifunctionality and Control of the Crumpling and Unfolding of Large-Area Graphene. *Nat Mater* **2013**, *12* (4), 321–325. https://doi.org/10.1038/nmat3542.

(34) Li, B.; Cao, Y.-P.; Feng, X.-Q.; Gao, H. Mechanics of Morphological Instabilities and Surface Wrinkling in Soft Materials: A Review. *Soft Matter* **2012**, *8* (21), 5728–5745. https://doi.org/10.1039/C2SM00011C.

(35) Yang, S.; Khare, K.; Lin, P.-C. Harnessing Surface Wrinkle Patterns in Soft Matter. *Adv. Funct. Mater.* **2010**, *20* (16), 2550–2564. https://doi.org/10.1002/adfm.201000034.

(36) Huntington, M. D.; Engel, C. J.; Hryn, A. J.; Odom, T. W. Polymer Nanowrinkles with Continuously Tunable Wavelengths. *ACS Appl. Mater. Interfaces* **2013**, *5* (13), 6438–6442. https://doi.org/10.1021/am402166d.

(37) Shao, Y.; Brook, M. A. Structured Metal Films on Silicone Elastomers. *J. Mater. Chem.* **2010**, *20* (39), 8548–8556. https://doi.org/10.1039/c0jm00824a.

(38) Breid, D.; Crosby, A. J. Effect of Stress State on Wrinkle Morphology. *Soft Matter* **2011**, *7* (9), 4490–4496. https://doi.org/10.1039/C1SM05152K.

(39) Matsuo, E. S.; Tanaka, T. Patterns in Shrinking Gels. *Nature* **1992**, *358* (6386), 482–485. https://doi.org/10.1038/358482a0.

(40) Li, Y.; Li, C.; Hu, Z. Pattern Formation of Constrained Acrylamide/Sodium Acrylate Copolymer Gels in Acetone/Water Mixture. *J. Chem. Phys.* **1994**, *100* (6), 4637–4644. https://doi.org/10.1063/1.466296.

(41) Guvendiren, M.; Burdick, J. A.; Yang, S. Solvent Induced Transition from Wrinkles to Creases in Thin Film Gels with Depth-Wise Crosslinking Gradients. *Soft Matter* **2010**, *6* (22), 5795–5801. https://doi.org/10.1039/C0SM00317D.

(42) Tanaka, T.; Sun, S.-T.; Hirokawa, Y.; Katayama, S.; Kucera, J.; Hirose, Y.; Amiya, T. Mechanical Instability of Gels at the Phase Transition. *Nature* **1987**, *325* (6107), 796–798. https://doi.org/10.1038/325796a0.

(43) Trujillo, V.; Kim, J.; Hayward, R. C. Creasing Instability of Surface-Attached Hydrogels. *Soft Matter* **2008**, *4* (3), 564–569. https://doi.org/10.1039/B713263H.

(44) Huraux, K.; Narita, T.; Bresson, B.; Frétigny, C.; Lequeux, F. Wrinkling of a Nanometric Glassy Skin/Crust Induced by Drying in Poly(Vinyl Alcohol) Gels. *Soft Matter* **2012**, *8* (31), 8075–8081. https://doi.org/10.1039/C2SM25480H.

(45) Guvendiren, M.; Burdick, J. A.; Yang, S. Kinetic Study of Swelling-Induced Surface Pattern Formation and Ordering in Hydrogel Films with Depth-Wise Crosslinking Gradient. *Soft Matter* **2010**, *6* (9), 2044–2049. https://doi.org/10.1039/B927374C.

(46) Liaw, C.-Y.; Pereyra, J.; Guvendiren, M. Chapter 9 Wrinkling on Covalently Anchored Hydrogels. In *Wrinkled Polymer Surfaces*; González-Henríquez, C. M., Rodríguez-Hernández, J., Eds.; Springer International Publishing: Cham, 2019; pp 205–227. https://doi.org/10.1007/978-3-030-05123-5_9.

(47) Wang, Q.; Zhao, X. A Three-Dimensional Phase Diagram of Growth-Induced Surface Instabilities. *Sci Rep* **2015**, *5* (1), 8887. https://doi.org/10.1038/srep08887.

(48) Kang, M. K.; Huang, R. Swell-Induced Surface Instability of Confined Hydrogel Layers on Substrates. *Journal of the Mechanics and Physics of Solids* **2010**, *58* (10), 1582–1598. https://doi.org/10.1016/j.jmps.2010.07.008.

(49) Han, Q.; Li, C.; Guan, Y.; Zhu, X. X.; Zhang, Y. Swelling-Induced Surface Instability of a Hydrogen-Bonded LBL Film and Its Self-Healing. *Polymer* **2014**, *55* (9), 2197–2204. https://doi.org/10.1016/j.polymer.2014.03.015.

(50) Breid, D.; Crosby, A. J. Surface Wrinkling Behavior of Finite Circular Plates. *Soft Matter* **2009**, *5* (2), 425–431. https://doi.org/10.1039/B807820C.

(51) Kim, H. S.; Crosby, A. J. Solvent-Responsive Surface via Wrinkling Instability. *Advanced Materials* **2011**, *23* (36), 4188–4192. https://doi.org/10.1002/adma.201101477.

(52) Basu, S. K.; McCormick, Alon. V.; Scriven, L. E. Stress Generation by Solvent Absorption and Wrinkling of a Cross-Linked Coating atop a Viscous or Elastic Base. *Langmuir* **2006**, *22* (13), 5916–5924. https://doi.org/10.1021/la060551o.

(53) Chung, J. Y.; Nolte, A. J.; Stafford, C. M. Diffusion-Controlled, Self-Organized Growth of Symmetric Wrinkling Patterns. *Advanced Materials* **2009**, *21* (13), 1358–1362. https://doi.org/10.1002/adma.200803209.

(54) Li, Y.; Peterson, J. J.; Jhaveri, S. B.; Carter, K. R. Patterned Polymer Films via Reactive Silane Infusion-Induced Wrinkling. *Langmuir* **2013**, *29* (14), 4632–4639. https://doi.org/10.1021/la400155d.

(55) Chung, J. Y.; Nolte, A. J.; Stafford, C. M. Surface Wrinkling: A Versatile Platform for Measuring Thin-Film Properties. *Advanced Materials* **2011**, *23* (3), 349–368. https://doi.org/10.1002/adma.201001759.

(56) Bowden, N.; Brittain, S.; Evans, A. G.; Hutchinson, J. W.; Whitesides, G. M. Spontaneous Formation of Ordered Structures in Thin Films of Metals Supported on an Elastomeric Polymer. *Nature* **1998**, *393* (6681), 146–149. https://doi.org/10.1038/30193.

(57) Cai, S.; Chen, D.; Suo, Z.; Hayward, R. C. Creasing Instability of Elastomer Films. *Soft Matter* **2012**, *8* (5), 1301–1304. https://doi.org/10.1039/C2SM06844C.

(58) González-Henríquez, C. M.; Sarabia Vallejos, M. A.; Rodríguez-Hernández, J. Chapter 2 Strategies for the Fabrication of Wrinkled Polymer Surfaces. In *Wrinkled Polymer Surfaces*; González-Henríquez, C. M., Rodríguez-Hernández, J., Eds.; Springer International Publishing: Cham, 2019; pp 19–59. https://doi.org/10.1007/978-3-030-05123-5_2.

(59) Gao, X.; Li, J.; Li, T.; Su, Z.; Ma, X.; Yin, J.; Jiang, X. Photo-Polymerization Induced Hierarchical Pattern via Self-Wrinkling. *Adv. Funct. Mater.* **2021**, *31* (49), 2106754. https://doi.org/10.1002/adfm.202106754.

(60) Hou, H.; Yin, J.; Jiang, X. Smart Patterned Surface with Dynamic Wrinkles. *Accounts Chem. Res.* **2019**, *52* (4), 1025–1035. https://doi.org/10.1021/acs.accounts.8b00623.

(61) Gan, Y.; Jiang, X.; Yin, J. Self-Wrinkling Patterned Surface of Photocuring Coating Induced by the Fluorinated POSS Containing Thiol Groups (F-POSS-SH) as the Reactive Nanoadditive. *Macromolecules* **2012**, *45* (18), 7520–7526. https://doi.org/10.1021/ma301439g.

(62) Rhee, D.; Deng, S.; Odom, T. W. Soft Skin Layers for Reconfigurable and Programmable Nanowrinkles. *Nanoscale* **2020**, *12* (47), 23920–23928. https://doi.org/10.1039/d0nr07054h.

(63) Lee, W.-K.; Jung, W.-B.; Rhee, D.; Hu, J.; Lee, Y.-A. L.; Jacobson, C.; Jung, H.-T.; Odom, T. W. Monolithic Polymer Nanoridges with Programmable Wetting

Transitions. *Adv. Mater.* **2018**, *30* (32), 1706657. https://doi.org/10.1002/adma.201706657.

(64) Thami, T.; Nasr, G.; Bestal, H.; Van der Lee, A.; Bresson, B. Fonctionalization of Surface-Grafted Polymethylhydrosikloxane with Alkyl Side Chains. *J. Polym. Sci. Part A: Polym. Chem.* **2008**, *46*, 3546–3562. https://doi.org/10.1002/pola.22691.

(65) Amro, K.; Clement, S.; Dejardin, P.; Douglas, W. E.; Gerbier, P.; Janot, J.-M.; Thami, T. Supported Thin Flexible Polymethylhydrosiloxane Permeable Films Functionalised with Silole Groups: New Approach for Detection of Nitroaromatics. *J. Mater. Chem.* **2010**, *20* (34), 7100–7103. https://doi.org/10.1039/c0jm01165g.

(66) Ferez, L.; Thami, T.; Akpalo, E.; Flaud, V.; Tauk, L.; Janot, J.-M.; Dejardin, P. Interface of Covalently Bonded Phospholipids with a Phosphorylicholine Head: Characterization, Protein Nonadsorption, and Further Functionalization. *Langmuir* **2011**, *27* (18), 11536–11544. https://doi.org/10.1021/la202793k.

(67) Thami, T.; Tauk, L.; Flaud, V. Controlled Structure and Hydrophilic Property of Polymethylhydrosiloxane Thin Films Attached on Silicon Support and Modified with Phosphorylcholine Group. *Thin Solid Films* **2020**, *709*, 138196. https://doi.org/10.1016/j.tsf.2020.138196.

(68) Thami, T.; Bresson, B.; Fretigny, C. Tailoring of Elastomeric Grafted Coating via Sol-Gel Chemistry of Crosslinked Polymethylhydrosiloxane. *J. Appl. Polym. Sci.* **2007**, *104* (3), 1504–1516. https://doi.org/10.1002/app.25295.

(69) Ameduri, B.; Boutevin, B.; Moreau, J. J. E.; Moutaabbid, H.; Chi Man, M. W. Hybrid Organic–Inorganic Gels Containing Perfluoro-Alkyl Moieties. *Journal of Fluorine Chemistry* **2000**, *104* (2), 185–194. https://doi.org/10.1016/S0022-1139(00)00211-6.

(70) Ameduri, B.; Boutevin, B.; Guida-Pietrasanta, F.; Manseri, A.; Ratsimihety, A.; Caporiccio, G. Synthesis of Hybrid Fluorinated Silicones. I. Influence of the Spacer between the Silicon Atom and the Fluorinated Chain in the Preparation and the Thermal Properties of Hybrid Homopolymers. *Journal of Polymer Science Part A: Polymer Chemistry* **1996**, *34* (15), 3077–3090. https://doi.org/10.1002/pola.1996.867.

(71) Doeff, M. M.; Lindner, E. Structure and Surface Energy Characteristics of a Series of Pseudo-Perfluoroalkyl Polysiloxanes. *Macromolecules* **1989**, *22* (7), 2951–2957. https://doi.org/10.1021/ma00197a013.

(72) Furukawa, Y.; Yoneda, T. Synthesis and Properties of Fluorosilicone with Perfluorooctylundecyl Side Chains. *Journal of Polymer Science Part A: Polymer Chemistry* **2003**, *41* (17), 2704–2714. https://doi.org/10.1002/pola.10817.

(73) Gupta, S. P.; Moreau, M.; Masure, M.; Sigwalt, P. Cationic Polymerization of 1,3,5,7 Tetramethylcyclotetrasiloxane Initiated by Trifluoromethanesulfonic Acid. *Eur. Polym. J.* **1993**, *29* (1), 15–22.

(74) Améduri, B.; Boutevin, B.; Nouiri, M.; Talbi, M. Synthesis and Properties of Fluorosilicon-Containing Polybutadienes by Hydrosilylation of Fluorinated Hydrogenosilanes. Part 1. Preparation of the Silylation Agents. *Journal of Fluorine Chemistry* **1995**, *74* (2), 191–197. https://doi.org/10.1016/0022-1139(95)03286-M.

(75) Dirany, M.; Dies, L.; Restagno, F.; Léger, L.; Poulard, C.; Miquelard-Garnier, G. Chemical Modification of PDMS Surface without Impacting the Viscoelasticity: Model Systems for a Better Understanding of Elastomer/Elastomer Adhesion and Friction. *Colloids and Surfaces A: Physicochemical and Engineering Aspects* **2015**, *468*, 174–183. https://doi.org/10.1016/j.colsurfa.2014.12.036.

(76) Bass, M.; Freger, V. Facile Evaluation of Coating Thickness on Membranes Using ATR-FTIR. *Journal of Membrane Science* **2015**, *492*, 348–354. https://doi.org/10.1016/j.memsci.2015.05.059.

(77) Scofield, J. H. Hartree-Slater Subshell Photoionization Cross-Sections at 1254 and 1487 EV. *Journal of Electron Spectroscopy and Related Phenomena* **1976**, *8* (2), 129–137. https://doi.org/10.1016/0368-2048(76)80015-1.

(78) Johnson, K. L.; Kendall, K.; Roberts, A. D.; Tabor, D. Surface Energy and the Contact of Elastic Solids. *Proceedings of the Royal Society of London. A. Mathematical and Physical Sciences* **1971**, *324* (1558), 301–313. https://doi.org/10.1098/rspa.1971.0141.

(79) Owens, D. K.; Wendt, R. C. Estimation of the Surface Free Energy of Polymers. *Journal of Applied Polymer Science* **1969**, *13* (8), 1741–1747. https://doi.org/10.1002/app.1969.070130815.

(80) Honda, K.; Morita, M.; Otsuka, H.; Takahara, A. Molecular Aggregation Structure and Surface Properties of Poly(Fluoroalkyl Acrylate) Thin Films. *Macromolecules* **2005**, *38* (13), 5699–5705. https://doi.org/10.1021/ma050394k.

(81) de Crevoisier, G.; Fabre, P.; Leibler, L.; Tencé-Girault, S.; Corpart, J. M. Structure of Fluorinated Side-Chain Smectic Copolymers: Role of the Copolymerization Statistics. *Macromolecules* **2002**, *35* (10), 3880–3888. https://doi.org/10.1021/ma010459t.

(82) Sheiko, S.; Lermann, E.; Möller, M. Self-Dewetting of Perfluoroalkyl Methacrylate Films on Glass. *Langmuir* **1996**, *12* (16), 4015–4024. https://doi.org/10.1021/la960229l.

(83) Gualandris, V.; Babonneau, F.; Janicke, M. T.; Chmelka, B. F. NMR Studies on Hydrolysis and Condensation Reactions of Alkoxysilanes Containing Si-H Bonds. *J. Sol-Gel Sci. Technol.* **1998**, *12*, 75–80.

(84) Loy, D. A.; Baugher, B. M.; Baugher, C. R.; Schneider, D. A.; Rahimian, K. Substituent Effects on the Sol-Gel Chemistry of Organotriakoxysilanes. *Chemistry of Materials* **2000**, *12*, 3624–3632.

(85) Hopcroft, M. A.; Nix, W. D.; Kenny, T. W. What Is the Young's Modulus of Silicon? *J. Microelectromech. Syst.* **2010**, *19* (2), 229–238. https://doi.org/10.1109/JMEMS.2009.2039697.

(86) Brook, M. A. *Silicon, in Organic, Organometallic and Polymer Chemistry*; John Wiley: New York, 1995.

(87) Nair, S. S.; Wang, C.; Wynne, K. J. AFM Peakforce QNM Mode for Measurement of Nanosurface Mechanical Properties of Pt-Cured Silicones. *Progress in Organic Coatings* **2019**, *126*, 119–128. https://doi.org/10.1016/j.porgcoat.2018.10.008.

(88) *Hydrosilylation: A Comprehensive Review on Recent Advances*; Marciniec, B., Ed.; Advances in Silicon Science; Springer Netherlands, 2009. https://doi.org/10.1007/978-1-4020-8172-9.

(89) Lukevics, E.; Belyakova, Z. V.; Pomerantseva, M. G.; Voronkov, M. G. Hydrosilylation. Recent Achievments. *J. Organomet. Chem. Libr.* **1977**, *5*, 1–179.

(90) Chruściel, J. J. Hydrosilyl-Functional Polysiloxanes: Synthesis, Reactions and Applications. In *Reactive and Functional Polymers Volume One : Biopolymers, Polyesters, Polyurethanes, Resins and Silicones*; Gutiérrez, T. J., Ed.; Springer International Publishing: Cham, 2020; pp 329–414.

(91) Améduri, B.; Boutevin, B.; Nouiri, M.; Talbi, M. Synthesis and Properties of Fluorosilicon-Containing Polybutadienes by Hydrosilylation of Fluorinated Hydrogenosilanes. Part 1. Preparation of the Silylation Agents. *Journal of Fluorine Chemistry* **1995**, *74* (2), 191–197. https://doi.org/10.1016/0022-1139(95)03286-M.

(92) Stein, J.; Lewis, L. N.; Gao, Y.; Scott, R. A. In Situ Determination of the Active Catalyst in Hydrosilylation Reactions Using Highly Reactive Pt(0) Catalyst

Precursors. *J. Am. Chem. Soc.* **1999**, *121* (15), 3693–3703. https://doi.org/10.1021/ja9825377.

(93) Zisman, W. A. Relation of the Equilibrium Contact Angle to Liquid and Solid Constitution. In *Contact Angle, Wettability, and Adhesion*; Advances in Chemistry; American Chemical Society, 1964; Vol. 43, pp 1–51. https://doi.org/10.1021/ba-1964-0043.ch001.

(94) Kobayashi, H.; Owen, M. J. Surface Tension of Poly[(3,3,4,4,5,5,6,6,6-Nonafluorohexyl)Methylsiloxane]. *Macromolecules* **1990**, *23* (23), 4929–4933. https://doi.org/10.1021/ma00225a008.

(95) Hozumi, A.; Takai, O. Effect of Hydrolysis Groups in Fluoro-Alkyl Silanes on Water Repellency of Transparent Two-Layer Hard-Coatings. *Applied Surface Science* **1996**, *103* (4), 431–441. https://doi.org/10.1016/S0169-4332(96)00534-X.

## For Table of Contents Only